TISSUE ENGINEERING
Volume 5, Number 3, 1999
Mary Ann Liebert, Inc.

In Vivo Measurement of Solute Transport Rates in a Bioartificial Organ

JULIE A. KROHN, M.S.,[1] ANDREW R. BAKER, M.S.,[1] JENNIFER L. LONG, B.S.,[2] RONALD L. FOURNIER, Ph.D.,[1] and JAMES P. BYERS, Ph.D.[1]

ABSTRACT

A radioactive tracer technique was used to evaluate the *in vivo* mass transfer properties of a tissue engineered bioartificial organ. To obtain these measurements, bioartificial organs were first implanted in ten rats and allowed to vascularize for 4 weeks. After vascularization, radioactive inulin was placed within the cell chamber of the device. Following the addition of tracer, blood samples were taken over a 4-h time period and inulin levels were determined. The results of these experiments were interpreted using a compartmental model that describes the transport of inulin from the cell chamber, across the immunoisolation membrane, and into the neovascularized region contained within the adjacent scaffold material. Nonlinear regression analysis of the plasma inulin levels using a four-compartment pharmacokinetic model provided estimates of the membrane permeability, the product of the capillary wall surface area and capillary permeability, and the glomerular filtration rate (GFR). The permeability of the membrane was found to be $3.50 \times 10^{-5} \pm 1.15 \times 10^{-5}$ cm/sec (95% confidence interval, $n = 10$), which compares favorably to previous *in vitro* permeability data for this membrane. The capillary wall permeability was found to be 0.0087 ± 0.0029 cm^3/sec/100 g of tissue. This compares well to a reported value for inulin of 0.01 cm^3/sec/100 g of tissue. The GFR was found to be 0.44 ± 0.07 ml/h/g BW, which compares well with a reported value of 0.40 ml/hr/g BW. The inulin tracer technique reported here is a useful tool for assessing the *in vivo* transport characteristics of a bioartificial organ as well as the vascularization within tissue engineered structures.

INTRODUCTION

BIOARTIFICIAL ORGANS ISOLATE TRANSPLANTED CELLS from the host's immune system using an immunoisolation membrane.[1–10] The transplanted cells have the ability to restore a lost function, for example, control of glucose levels, through either secretion of the needed therapeutic agent, or by consuming a metabolite. The immunoisolation membrane protects the cells from the host's immune system. This membrane is permeable to small molecules such as required nutrients and the therapeutic agent released by the cells, but impermeable to the larger molecules (antibodies and complement) and cells of the host's immune

[1]Department of Bioengineering, The University of Toledo, Toledo, Ohio.
[2]Department of Chemical Engineering, The University of Toledo, Toledo, Ohio.

system. Techniques for measuring the permeability of solutes through immunoisolation membranes have been described.[4,6,7] These devices are also known as hybrid artificial organs because they consist of both artificial materials and living tissue or cells.

Solute transport between the surrounding vasculature and the immunoprotected cells within a bioartificial organ is critical to maintain viability and the therapeutic function of the transplanted cells. Furthermore, an understanding of *in vivo* solute transport is needed for the rational design and scale-up of these devices. In many cases, this information is not easily determined when the therapeutic cells themselves are being used. This is because it is difficult to obtain first-hand information on cell viability and cellular responsiveness in terms of the solute release or consumption rate. Solute transport for a bioartificial organ will also depend on many environmental factors, which include the solute concentration within the device and in the local blood supply, the number and proximity of the blood vessels that are in the neighborhood of the implant, the solute permeability of the immunoisolation membrane, the solute production or consumption rate of the cells, the geometry of the implanted device, and the spatial arrangement and density of the immunoprotected cells.[2,3,5]

In this study, we report on the evaluation of the mass transport characteristics of the planar bioartificial organ shown in Figure 1. The immunoisolation membrane used in this study was developed in a previous study[6] and comprises a microporous polyether sulfone (PES) filter and a high water content polyvinyl alcohol (PVA) hydrogel.[11]

One of the unique aspects of the device evaluated in this study was the development of a neovascularized region.[8,12–16] Tissue engineering concepts were used to encourage vascularized in-growth of tissue in a scaffold material adjacent to the immunoisolation membrane. Vascularization of the scaffold material next to the implant is important before implantation of cells to ensure proper transport of nutrients and waste products between the implant and the body. Prevascularization of the region next to the implant prior to cell seeding will optimize the mass transport needed for the exchange of nutrients and wastes.[16–19] This will increase the likelihood that the cells will survive and perform their desired function.

The mass transfer characteristics of the capillary bed and immunoisolation membrane were measured by using a radioactive tracer technique.[16] Radioactive inulin was used as the tracer molecule in these experiments. This polysaccharide molecule has a molecular weight of approximately 5,500 D. Inulin is an ideal choice for a tracer because it is simply filtered in the glomerulus and is neither absorbed nor secreted in the renal tubules. Furthermore, it is not metabolized by the body.[20,21] This allows a relatively simple analysis using a compartmental model to determine the inulin transport kinetics from the bioartificial organ and its elimination from the body. The use of radioactive inulin therefore allows for the development of a quantitative description of the solute transport between the implant and body. This allowed for determination of the permeability of the membrane, the product of the capillary permeability and the surface area of the capillary wall, and the glomerular filtration rate.

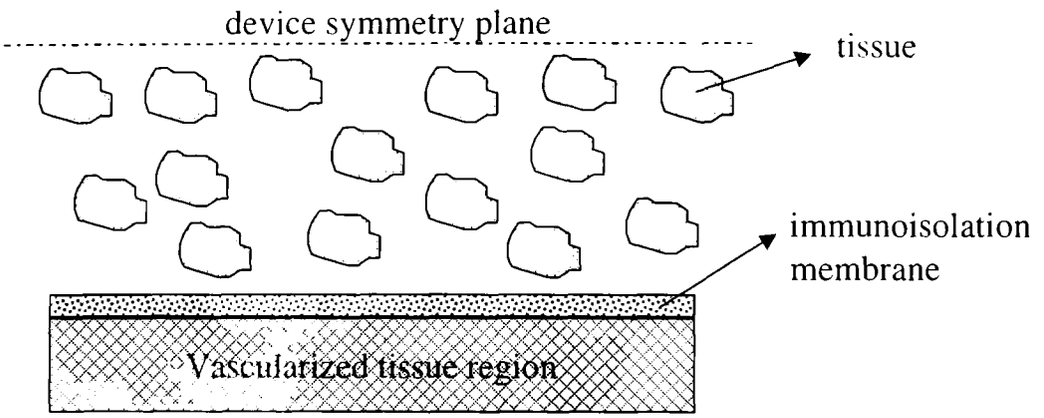

FIG. 1. Diagram of cell transplantation device after implantation and neovascularization of polymer scaffold.

MATERIALS AND METHODS

Animals

The experiments were conducted using 340–460 g male Harlan-Sprague-Dawley rats (n = 10). The protocols for all animal procedures were reviewed and approved by the animal usage committees of both The University of Toledo and the Medical College of Ohio. The animals were supplied with unlimited rat chow and water throughout the study.

Membrane and Device Preparation

The membranes and the methods used to prepare them were the same as those described in Baker et al.[6] The membranes were made of a microporous PES filter impregnated with a PVA hydrogel. The preparation of the PVA solution was similar to that described in Inoue et al.[11] The PVA (Aldrich, 9–10 kd average MW, 80% hydrolyzed, Milwaukee, WI) hydrogel was prepared by adding 0.3 g PVA to 8.71 ml distilled water. This mixture was vigorously stirred at room temperature for several hours until thoroughly mixed. Additions of 984 μl of 1.0 N HCl and 15 μl of glutaraldehyde (GA) (Aldrich, 50 wt%, Milwaukee, WI) were then mixed into the solution. This solution produced a 3 wt% PVA solution of 0.1 N HCl and 0.083% GA. The PES filters (Gelman, 0.2 μm Supor-200, Ann Arbor, MI) were soaked in the polymer solution until completely wetted. The filters were placed on a polypropylene rack and allowed to gel at 37°C/90% humidity. To ensure the pores of the PES filter were completely wetted and gelled with the PVA solution, the process was repeated three times, 24 hours apart. To remove the unwanted acid and unreacted GA, the membranes were boiled in distilled water for 30 minutes. The membranes were stored at room temperature in distilled water or normal saline until use.

The device was then assembled by placing a layer of an artificial scaffold material (Polyester Surgical Support Felt, Meadox Medicals, Inc., Oakland, NJ) next to the immunoisolation membrane as shown in Figure 1. The scaffold was treated with collagen and acidic fibroblastic growth factor (aFGF) to promote vascularization according to the procedure described by Thompson et al.[19]

Device Implantation

The rats were anesthetized by an intramuscular injection of ketamine (35 mg/kg body weight, Aveco Co., Inc., Ford Dodge, IA) and xylazine (7 mg/kg body weight, Mobay Corp., Shawnee, KS). Using sterile technique, a 1.5-inch midline incision was made through the skin and abdominal wall. The bioartificial device was anchored to the muscle of the abdominal wall with two sutures. The scaffold material was positioned to be in direct contact with the omentum directly below the liver. Two to three stitches were made through the omentum to ensure the source of vascularization was from the omentum. Two final stitches were made to attach the device to the abdominal wall. The incision in the abdominal wall was closed using 4-0 chromic gut absorbable sutures. The incision in the skin was closed using 4-0 silk nonabsorbable sutures. The incision site was washed with Betadine (Purdue Frederick, Norwalk, CN) and the animal was placed in a clean cage, on a heating pad, to recover.

Inulin Tracer Injection Experiments

In a previous study,[16] we examined the degree of vascularization of the surgical support felt as a function of time. In that study we used histology, radioactive microspheres, and the inulin tracer technique to assess vascularization. We found that 28 days is more than enough time to completely vascularize the surgical support felt. The inulin tracer studies reported here were therefore performed after allowing 28 days for device vascularization. The studies described here also used the much more permeable membrane developed by Baker et al.[6]

The radioactive inulin (^{14}C-methylated, β-particle emitter, 10.3 μCi/mg) tracer solution was prepared the day of the experiment by thoroughly mixing 25 μCi of crystalline solid radioactive inulin (Sigma Chemical Co., St. Louis, MO) in 0.7 ml of sterile-filtered isotonic saline (0.9% NaCl by weight).[16] An intraperitoneal injection of sodium pentobarbital (65 mg/kg body weight, The Butler Company, Columbus, OH) was used to anesthetize the animal and the right femoral artery and vein was cannulated. A background sample

was provided by a 100 μl blood sample collected from the arterial catheter. The inlet port and implantation device were flushed with saline and the remaining saline solution was displaced with air. A syringe containing 200 μl of the inulin solution was slowly injected into the inlet port of the device over a period of 20 sec. Silicone tubing was attached to the outlet port to collect the excess tracer solution and prevent radioactive contamination of the animal's skin. Following injection, the silicone tubing on the outlet port was clamped to prevent backflow.

After tracer injection, blood samples were collected from the arterial catheter at 10, 30, 60, 90, 120, 150, 180, 210, and 240 min. To make sure the catheter was filled with fresh blood, 0.05 ml of fluid was withdrawn from the arterial catheter prior to each sample. A blood sample of 0.1 ml was then collected with a new syringe. To remove any residual blood from the catheter and replace lost fluid volume from sampling, the arterial catheter was flushed with 0.15 ml of sterile isotonic saline. After the last blood sample was collected, the device chamber was flushed with 1.0 ml of saline to remove any remaining radioactive tracer.

The blood samples were centrifuged at 5000 rpm for 5 min. The supernatant was removed from each sample and then mixed with 3.5 ml of deionized water and 11.5 ml of Universol scintillation cocktail (ICN Radiochemicals, Irvine, CA) in a borosilicate glass scintillation vial. A sample of inulin injection solution was similarly prepared after 1:100 dilution in saline. A Packard Tri-Carb 4530 automated liquid scintillation counter (Packard Instrument Co., Meriden, CT) was used to measure the radioactive levels of all samples.

The plasma inulin concentrations were converted to dimensionless form. This allowed comparable concentrations between the animals by eliminating differences in body distribution volumes (V_B) and initial dose (D). The dimensionless concentrations (X) were calculated by the following equation:

$$X = \frac{C}{\left(\frac{D}{V_B}\right)} \tag{1}$$

where C represents the measured plasma inulin concentration and D is the total dose of radioactive inulin injected into the device at the start of the experiment. The denominator of this equation denotes the maximum possible plasma inulin level that would occur if the inulin dose was assumed to be instantly mixed throughout the distribution volume at the time of injection. Therefore, the dimensionless concentration is constrained between values of zero and one.

Pharmacokinetic Analysis of Tracer Concentration

The four-compartment pharmacokinetic model shown in Figure 2 was used to analyze the data collected from the inulin injection experiments. The compartmental model describes the distribution of inulin in the implantation device and the body. The first three compartments are used to describe transport within the implantation device. The first compartment consists of the implantation chamber that is initially injected with inulin. The inulin is assumed to diffuse from this first compartment across the immunoisolation membrane, and into the second compartment, which is represented by the extracellular fluid of the scaffold tissue. Within this scaffold tissue is the third compartment, the capillary bed. The inulin diffuses from the scaffold tissue into the capillaries that have a blood flow rate, Q_{CB}. Inulin is transported to the body, or fourth compartment, via the blood flow in the matrix capillaries. In the fourth compartment, inulin is removed from the body by filtration through the kidneys. The equations describing the relationships between these compartments are given by the following four differential equations.

$$V_I \frac{dX_I}{dt} = -P_M S_M (X_I - X_T) \tag{2}$$

$$V_T \frac{dX_T}{dt} = P_M S_M (X_I - X_T) - P_{CW} S_{CW} (X_T - X_C) \tag{3}$$

$$V_C \frac{dX_C}{dt} = Q_{CB} (X_B - X_C) + P_{CW} S_{CW} (X_T - X_C) \tag{4}$$

$$V_B \frac{dX_B}{dt} = -Q_{CB} (X_B - X_C) - GFR \times X_B \tag{5}$$

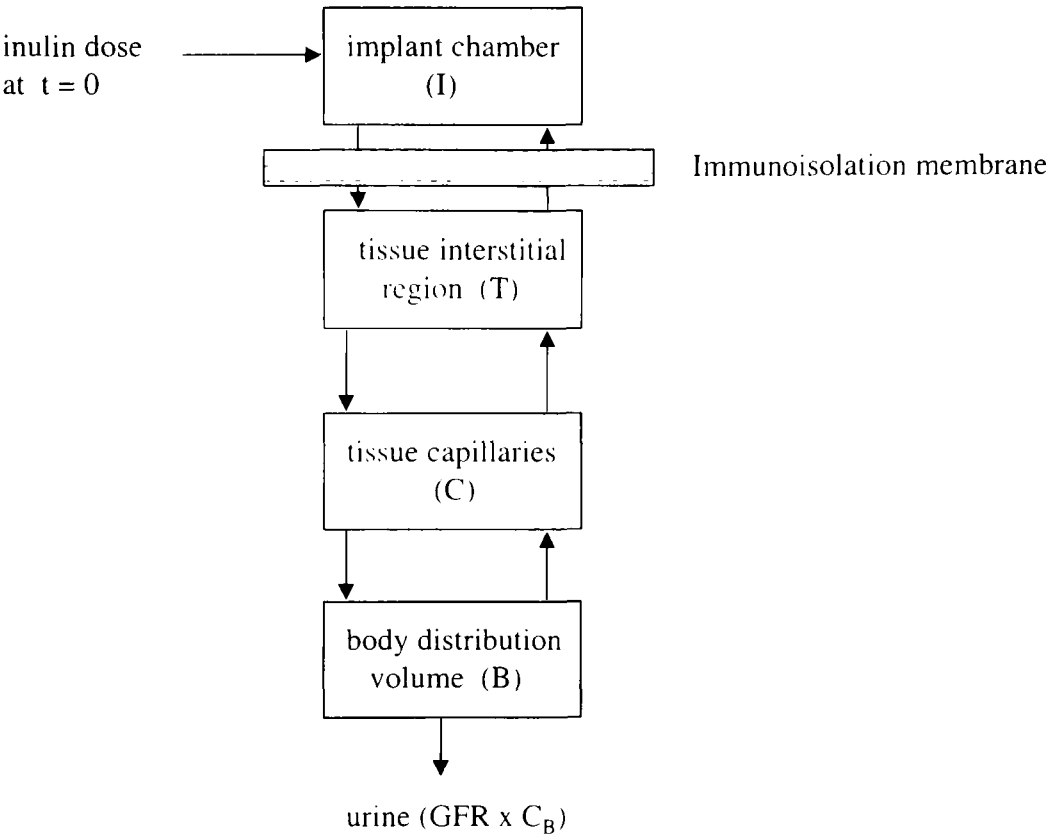

FIG. 2. Four-compartment pharmacokinetic model for analysis of plasma inulin concentrations.

The initial conditions of the equations at t = 0 are $X_I = V_B/V_I$ and $X_T = X_C = X_B = 0$. Table 1 presents a list and description of the variables used in the compartmental model shown above. In the above equations, P_M and P_{CW} are the permeabilities of the immunoisolation membrane and the capillary wall, respectively. We assume that these are controlling resistances for the transport of inulin from the device into the capillaries within the matrix.

Because the inulin concentration measurements were based on plasma volume, the blood flow rate through the tissue region (Q_{CB}) needs to be adjusted to account for the extracellular volume fraction of blood, ζ_C.[16,22] If the inulin concentration measurements were based on the total blood volume, ζ_C would be equal to one. The volume of the implantation chamber (V_I) is determined from the given device dimensions. V_T represents the tissue region extracellular fluid volume and is equivalent to $f_T\zeta_T S_M \delta_T \epsilon_M$. The void fraction of the support structure is represented by ϵ_M, the fraction of support structure void volume that contains tissue is f_T, and the support structure thickness is δ_T. Inulin only distributes within the extracellular fluid space in the tissue region. The extracellular volume fraction of the tissue (ζ_T) is about 0.15 for most tissues.[26–28] This fluid surrounding the cells is also assumed to be well mixed and the inulin concentration homogenous. The capillary volume (V_C) in the tissue region is given by $vf_T S_M \delta_T \epsilon_M$, where v is the capillary volume fraction. The capillary volume fraction for this scaffold material at 28 days was found to be 0.23%.[16] Other parameters are defined in Table 1.

Two simplifications of equations 2–5 can be made. First, the capillary volume (V_C) is assumed to be much smaller than the other volumes in the model. Therefore, the left-hand side of equation 4 tends to be very small and close to zero. Subsequently, the solute concentration in the capillary approaches a pseudo-steady state condition and an algebraic equation can be written to replace equation 4.

$$Q_{CB}(X_B - X_C) + P_{CW}S_{CW}(X_T - X_C) = 0 \tag{6}$$

The second simplification takes advantage of the fact that the solute concentration in the body (X_B) is much smaller than the solute concentration within the tissue capillaries of the implant device (X_C). Thus,

TABLE 1. PHARMACOKINETIC MODEL PARAMETER VALUES DETERMINED FROM LITERATURE OR FROM IMPLANT DEVICE DIMENSIONS

Term	*Value*	*Parameter description*
Basic Definitions		
C		Plasma inulin concentration
D		Inulin dose to device chamber
GFR		Glomerular filtration rate
K_{CW}		Constant defined by eqn. 7
P		Permeability
Q_{CB}		Scaffold capillary blood flow rate
S		Surface area
t		Time
V		Inulin distribution volume
X		dimensionless inulin concentration, eqn. 1
		As subscripts: (B) body, (C) scaffold capillaries, (CW) capillary wall, (I) implant chamber, (M) membrane, (T) scaffold tissue extracellular fluid
Measured Parameters Based on Literature or Device Dimensions		
f_T	1.0	Fraction of support structure void volume that contains tissue
Q_{CB}	0.056 ml/min	Tissue region blood flow rate[16]
r_c	3.6×10^{-4} cm	Capillary radius[16]
r_M	0.5 cm	Membrane radius
V_B	0.231 ml/g BW	Inulin body distribution volume[16]
V_I	0.083 ml	Volume of implantation chamber
δ_T	0.15 cm	Scaffold material thickness
δ_I	0.07 cm	Depth of implantation chamber
ϵ_M	0.84	Scaffold material void fraction
ζ_C	0.63	Extracellular void fraction of capillary blood[16,22]
ζ_T	0.15	Extracellular volume fraction of tissue[23–25]

the solute becomes significantly diluted when it enters the body compartment because the volume of the body compartment is several orders of magnitude larger than that of the capillaries within the device's scaffold structure. Therefore, rearrangement of equation 6 will provide the solute capillary concentration within the tissue region in terms of the solute concentration in the tissue compartment only.

$$X_C = \left[\frac{P_{CW}S_{CW}}{Q_{CB} + P_{CW}S_{CW}}\right] X_T = K_{CW}X_T \tag{7}$$

Additionally, equation 7 shows that the capillary solute concentration is essentially at equilibrium with the tissue solute concentration as given by the constant distribution coefficient, K_{CW}. Equations 2, 3, and 5, can be rewritten using equation 7 for the capillary concentration and then solved analytically using Laplace transforms to provide the following equations for the dimensionless solute concentrations in the implantation chamber, tissue region, and within the body compartment.[26,27]

$$X_I = \left[\frac{V_B(\lambda_1 - k_{TI} - k_{CW})}{V_I(\lambda_1 - \lambda_1)}\right] e^{-\lambda_1 t} + \left[\frac{V_B(\lambda_2 - k_{TI} - k_{CW})}{V_I(\lambda_2 - \lambda_1)}\right] e^{-\lambda_2 t} \tag{8}$$

$$X_T = \left[\frac{V_B k_{IT}}{V_T(\lambda_1 - \lambda_2)}\right](e^{-\lambda_2 t} - e^{-\lambda_1 t}) \tag{9}$$

$$X_B = \left[\frac{k_{IT}k_{CW}}{(\lambda_1 - \lambda_2)(\lambda_1 - k_{TE})}\right]e^{-\lambda_1 t} + \left[\frac{k_{IT}K_{CW}}{(\lambda_2 - \lambda_1)(\lambda_2 - k_{TE})}\right]e^{-\lambda_2 t} + \left[\frac{k_{IT}k_{CW}}{(k_{TE} - \lambda_1)(k_{TE} - \lambda_2)}\right]e^{-k_{TE}t} \quad (10)$$

The rate constants (k's) and constants λ_1 and λ_2 are given by the following equations.

$$k_{IT} = \frac{P_M S_M}{V_I} \quad (11)$$

$$k_{TI} = \frac{P_M S_m}{V_T} \quad (12)$$

$$k_{CW} = -\frac{P_{CW}S_{CW}(K_{CW} - 1)}{V_T} = \frac{Q_{CB}K_{CW}}{V_T} \quad (13)$$

$$k_{TE} = \frac{GFR}{V_B} \quad (14)$$

$$\lambda_1 = \frac{1}{2}\left[k_{IT} + k_{TI} + k_{CW} + \sqrt{(k_{IT} + k_{TI} + k_{CW})^2 - 4k_{IT}k_{CW}}\right] \quad (15)$$

$$\lambda_2 = \frac{1}{2}\left[k_{IT} + k_{TI} + k_{CW} - \sqrt{(k_{IT} + K_{TI} + k_{CW})^2 - 4k_{IT}k_{CW}}\right] \quad (16)$$

The pharmacokinetic model described above was used to evaluate data collected on ten rats with devices implanted for 28 days. Table 1 summarizes known values of the parameters based either on device dimensions or accepted literature values. The unknown parameters in the model are then (1) the membrane permeability (P_M), (2) the product of the capillary wall surface area and permeability (PS_{CW}), and (3) the glomerular filtration rate (GFR). These three parameters were estimated by performing a nonlinear regression on the inulin tracer data obtained following injection of the tracer into the chamber of the implantation device. Mathcad® (Mathsoft, Inc., Cambriole, MA) 7.0 was used to perform the nonlinear regression analysis. Mathcad uses the Levenberg-Marquardt method. The Mathcad tolerance variable (TOL) was reduced until there was no significant improvement in the resulting values of the three regression parameters.

RESULTS

A representative example of how the model fit the data for a given rat is illustrated in Figure 3. As shown in this figure, the pharmacokinetic model provided a good representation of the data. The values of the membrane permeability, product of the capillary wall surface area and permeability, and glomerular filtration rate were calculated for each rat and the averages of these values were determined within 95% confidence levels (n = 10). The membrane permeability was found to be $3.50 \times 10^{-5} \pm 1.15 \times 10^{-5}$ cm/sec and the product of the capillary wall surface area and permeability was estimated to be 0.0087 ± 0.0029 cm^3/sec/100 g of tissue. The average of the glomerular filtration rate was calculated to be 0.44 ± 0.07 mL/h/g of body weight.

DISCUSSION

Favorable solute transport rates between the implant and the host vasculature are required to maintain cell viability within a bioartificial organ. A radioactive inulin tracer technique was used in this study to quantitatively measure the *in vivo* mass transport rates within a bioartificial organ. Devices were implanted into ten rats for a period of 28 days to allow for vascularization and tissue ingrowth into the scaffold material adjacent to the immunoisolation membrane. A four compartment pharmacokinetic model was used to

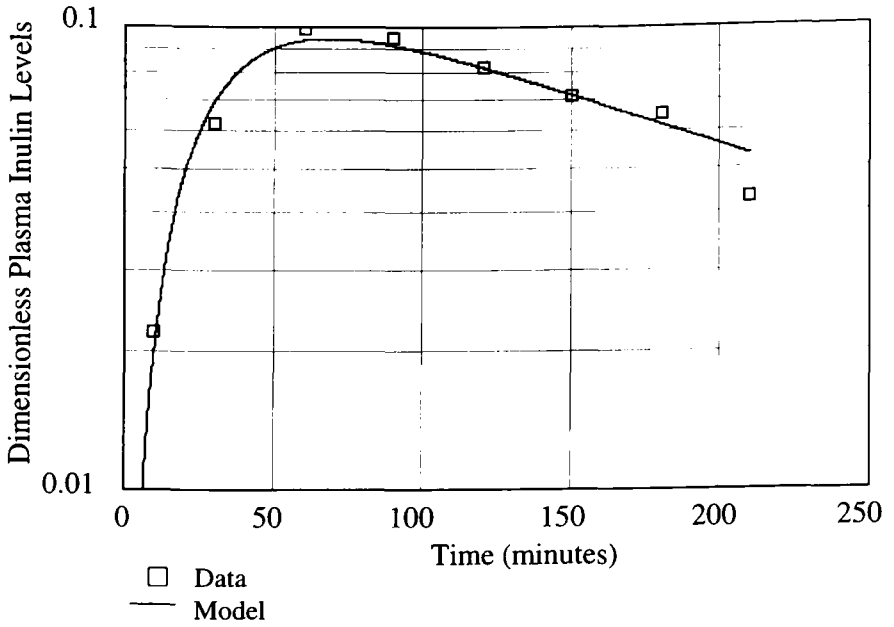

FIG. 3. Dimensionless plasma tracer concentration versus time after tracer injection into device chamber implanted in a rat for 28 days.

determine the membrane permeability (P_M), capillary wall surface area and permeability product (PS_{CW}), and the glomerular filtration rate (GFR). The results obtained from the pharmacokinetic model analysis are compared with previously reported data as summarized in Table 2. The model provided a good representation of the measured tracer concentration data and the overall results for ten rats shown in Table 2 compare well with literature values.

The immunoisolation membrane used in this experiment was previously analyzed by both *in vitro* and *in vivo* experiments. From Baker et al.,[6] an *in vitro* permeability (P_M) of inulin through the membrane was measured to be approximately 7.0×10^{-5} cm/sec. The membranes in that study were also implanted in rats for periods up to 180 days and then removed to analyze their permeability *in vitro*. The measured permeabilities of inulin in the removed *in vivo* membranes were found to range between 3.0×10^{-5} at 28 days to 6.5×10^{-5} cm/sec at 180 days. The permeability initially dropped at the beginning of the implantation period between 7 and 28 days. This reduction was hypothesized to have been caused by the wound healing process, supported by gross and microscopic signs of inflammation (unpublished observations). How-

TABLE 2. COMPARISON OF PERMEABILITIES AND GLOMERULAR FILTRATION RATES OBTAINED FROM THIS STUDY (n = 10) WITH REPORTED LITERATURE VALUES

	Values measured in this study after 28 days of implantation	*Values reported in various literature sources*
In vivo permeability of membrane, (P_M), (cm/sec)	$3.50 \times 10^{-5} \pm 1.15 \times 10^{-5}$	3.0×10^{-5} at 28 days[6] 6.5×10^{-5} at 180 days
Capillary surface area and permeability product, (PS_{CW}), (cm^3/sec/100 g tissue)	0.0087 ± 0.0029	0.01[28]
Glomerular filtration rate, (GFR), (ml/h/g BW)	0.44 ± 0.07	0.45 ± 0.02[16] 0.4[29]

ever, after 90 days, the permeability increased to 6.5×10^{-5} cm/sec and was maintained throughout the remainder of the 180 day experiment.

The membrane permeability obtained from the inulin experiments reported here was calculated to be $3.50 \times 10^{-5} \pm 1.15 \times 10^{-5}$ cm/sec. This value corresponds well with both the *in vitro* (7×10^{-5} cm/sec) and *in vivo* (3.0×10^{-5} cm/sec, at 28 days) permeabilities of the membrane reported in the Baker et al.[6] study. The lower *in vivo* permeability in these experiments is most likely a result of protein adsorption.[30,31] The product of the capillary wall permeability and surface area (PS_{CW}) was calculated from this study to be 0.0087 ± 0.0029 cm^3/sec/100 g of tissue. According to previously reported data,[28] inulin has a permeability and surface area product of approximately 0.01 cm^3/sec/100 g of tissue. The GFR was determined to be 0.44 ± 0.07 ml/h/g body weight in our study. This compares well with reported literature values for rats of 0.45 ± 0.02 ml/h/g body weight by Sarver et al.[16] and a typical value of 0.4 ml/h/g body weight.[29] Allowing for biological variations among the individual rats, the results obtained in this study agree well with previous data collected for values of membrane permeability, capillary wall surface area and permeability, and glomerular filtration rate. The fact that these measured *in vivo* values agree with these previous measurements supports the assumptions used to develop the four-compartment pharmacokinetic model described earlier.

The method of using a tracer technique to measure *in vivo* mass transport rates is a useful tool to assess the transport characteristics of a bioartificial organ as well as the vascularization within tissue engineered structures. This method could assist in the rational design of scaffold structures for tissue engineering applications, assist in device scale-up studies, as well as for determining the length of time required before the implantation of cells.

ACKNOWLEDGMENTS

This work was supported by grants from the Juvenile Diabetes Foundation and SenMed Medical Ventures.

REFERENCES

1. Lanza, R.P., W.M. Kuhtreiber, and W.L. Chick. Encapsulation technologies. Tissue Eng. **1,** 181–196, 1995.
2. Colton, C.K. Implantable biohybrid artificial organs. Cell Transplant. **4,** 415–436, 1995.
3. Colton, C.K., and Avgoustiniatos, E.S. Bioengineering in development of the hybrid artificial pancreas. J. Biomech. Eng. **113,** 152–170, 1991.
4. Dionne, K.E., Cain, B.M., Li, R.H., Bell, W.J., Doherty, E.J., Rein, D.H., Lysaght, M.J., and Gentile, F.T. Transport characterization of membranes for immunoisolation. Biomaterials. **17,** 257–266, 1996.
5. Avgoustiniatos, E.S., and C.K. Colton. 1997. Design considerations in immunoisolation. In Principles of Tissue Engineering. Ed. R.P. Lanza, R. Langer, and W.L. Chick. 333-346. R.G. Landes Co. Boulder, CO.
6. Baker, A.R., Fournier, R.L., Sarver, J.G., Long, J.L., Goldblatt, P.J., Horner, J.M., Selman, S.T. Evaluation of an immunoisolation membrane formed by incorporating a polyvinyl alcohol hydrogel within a microporous filter support. Cell Transplant. **6,** 585–595, 1997.
7. Boyd, R.F., Lopez, M., Stephens, C.L., Velez, G.M., Ramirez, C.A., and Zydney, A.L. Solute washout experiments for characterizing mass transport in hollow fiber immunoisolation membranes. Ann. Biomed. Eng. **26,** 618–626, 1998.
8. Suzuki, K., Bonner-Weir, S., Hollister-Lock, J., Colton, C.K., and Weir, G.C. Number and volume of islets transplanted in immunobarrier devices. Cell Transplant. **7,** 47–52, 1998.
9. Lanza, R.P., Sullivan, S.J., and Chick, W.L. Islet transplantation with immunoisolation. Diabetes **41,** 1503–1510, 1992.
10. Lysaght, M.J., Frydel, B., Gentile, F.T., Emerich, D.F., and Winn, S.R. Recent progress in immunoisolated cell therapy. J. Cell. Biochem. **56,** 196–203, 1994.
11. Inoue, K., Fujisato, T., Gu, Y.J., Burczak, K., Sumi, S., Kogire, M., Tobe, T., Uchida, K., Nakai, I., Maetani, S., and Ikada, Y. Experimental hybrid islet transplantation: Applications of polyvinyl alcohol for entrapment of islets. Pancreas **7,** 562–568, 1992.
12. Brauker, J., Martnson, L.A., Loudovaris, T., Hill, R.S., Carr-Brendel, V., Hodgson, R., Young, S., Mandel, T.E.,

Charlton, B., and Johnson, R.C. Immuno-isolation with large pore membranes: Allografts are protected under conditions that result in destruction of xenografts. Cell Transplant. **1,** 164, 1992.
13. Brauker, J.H., Carr-Bendel, V.E., Martinson, L.A., Crudele, J., Johnston, W.D., and Johnson, R.C. Neovascularization of synthetic membranes directed by membrane microarchitecture. J. Biomed. Mater. Res. **29,** 1517–1524, 1995.
14. Brauker, J., Martinson, L.A., Young, S.K., and Johnson, R.C. Local inflammatory response around diffusion chambers containing xenografts. Transplantation **61,** 1671–1677, 1996.
15. Hill, R.S., Young, S.K., Jacobs, S.A., Martinson, L.A., and Johnson, R.C. Membrane encapsulated islets implanted in epididymal fat pads correct diabetes in rats. Cell Transplant. **1,** 168, 1992.
16. Sarver, J.G., Fournier, R.L., Goldblatt, P.J., Phares, T.L., Mertz, S.E., Baker, A.R., Mellon, R.J., Horner, J.M., and Selman, S.H. Tracer technique to measure in vivo chemical transport rates within an implantable cell transplantation device. Cell Transplant. **4,** 201–217, 1995.
17. Cima, L.G., Vacanti, J.P., Vacanti, C., Ingber, D., Mooney, D., and Langer, R. Tissue engineering by cell transplantion using degradable polymer substrates. J. Biomech. Eng. **113,** 143–151, 1991.
18. Stagner, J.I., and Samols, E. The induction of capillary bed development by endothelial cell growth factor before islet transplantation may prevent islet ischemia. Transpl. Proc. **22,** 824–828, 1990.
19. Thompson, J.A., Haudenschild, C.C., Anderson, K.D., DiPieto, J.M., Anderson, W.F., and Maciag, T. Heparin-binding growth factor 1 induces the formation of organoid neovascular structures in vivo. Proc. Natl. Acad. Sci. **86,** 7928–7932, 1989.
20. Henry, R.J., Cannon, D.C., Winkelman, J.W. In: Clinical Chemistry. 2nd ed. New York: Harper & Row, 1974, pp. 1312–1325.
21. Klaassen, C.D. Distribution, excretion, and absorption of toxicants. In: Casarett and Doull's toxicology: The basic science of poisons. 3rd ed., edited by J. Doull, C.D. Klaassen, and M.O. Amdur. New York: Macmillan Publishing Company, 1986, pp. 33–63.
22. Baker, H.J., Lindsey, J.R., and Weisbroth, S.H. In: The Laboratory Rat. New York: Academic Press, Inc., 1979, pp. 411–412.
23. Addanki, S., Cahill, F.D., and Sotos, J.F. A method for the determination of extracellular space with 3H inulin. Clin. Chem. **13,** 953–957, 1967.
24. Cooney, D.O. In: Biomedical engineering principles. New York: Marcel Dekker, Inc., 1976, pp. 21–75.
25. Pittman, J.A., and Debons, A.F. Thyroidal extracellular fluid compartments. Am. J. Physiol. **210,** 399–403, 1966.
26. Fournier, R.L. In: Basic Transport Phenomena in Biomedical Engineering. Taylor and Francis, Inc., 1999, Philadelphia.
27. Gibaldi, M. and Perrier, D. In: Parmacokinetics, 2nd ed. Marcel Dekker, Inc., 1982.
28. Renkin, E.M., and Curry, F.E. Transport of water and solutes across capillary endothelium. In: Membrane Transport in Biology, volume 4, edited by G. Giebisch and D. C. Tosteson. Springer-Verlag, 1979, pp. 1–45.
29. Durbin, P.W., and Schmidt, C.T. Predicting the kinetics of chelating agents in man from animal data. Health Phys. **57**(Suppl 1), 165–174, 1989.
30. Opong, W.S., and Zydney, A.L. Diffusive and convective protein transport through asymmetric membranes. AIChE J. **37,** 1497–1510, 1991.
31. Robertson, B.C., and Zydney, A.L. Protein adsorption in asymmetric ultrafiltration membranes with highly constricted pores. J. Col. Int. Sci. **134,** 563–575, 1990.

Address reprint requests to:
Ronald L. Fournier, Ph.D.
Department of Bioengineering
The University of Toledo
2801 W. Bancroft St.
Toledo, OH 43606

rfouri@uoft02.utoledo.edu